Topological remodeling of cortical perineuronal nets in focal cerebral ischemia and mild hypoperfusion

Egor Dzyubenko[a,b], **Daniel Manrique-Castano**[a,c,d], **Christoph Kleinschnitz**[a], **Andreas Faissner**[b †] **and Dirk M. Hermann**[a,†]

a - Department of Neurology, *University Hospital Essen, Hufelandstraße 55, D-45122 Essen, Germany*
b - Department of Cell Morphology and Molecular Neurobiology, *Faculty of Biology and Biotechnology, Ruhr University Bochum, D-44801 Universitätsstraße 150, Bochum, Germany*
c - International Graduate School of Neuroscience, *Ruhr University Bochum, D-44801 Universitätsstraße 150, Bochum, Germany*
d - Graduate School of Biomedical Science, *University of Duisburg-Essen, D-45147 Virchowstraße 179, Essen. Germany*

Correspondence to Andreas Faissner and Dirk M. Hermann: *A. Faissner, Department of Cell Morphology and Molecular Neurobiology, Faculty of Biology and Biotechnology, Ruhr University Bochum, D-44801 Universitätsstraße 150, Bochum, Germany. D. M. Hermann, Chair of Vascular Neurology, Dementia and Ageing Research, Department of Neurology, University Hospital Essen, Hufelandstraße 55, D-45122 Essen, Germany. andreas.faissner@rub.de.*
https://doi.org/10.1016/j.matbio.2018.08.001

Abstract

Despite the crucial role of perineuronal nets (PNNs) in neural plasticity and neurological disorders, their ultrastructural organization remains largely unresolved. We have developed a novel approach combining superresolution structured illumination microscopy (SR-SIM) and mathematical reconstruction that allows for quantitative analysis of PNN topology. Since perineuronal matrix is capable to restrict neural plasticity but at the same time is necessary to maintain synapses, we hypothesized that a beneficial post stroke recovery requires a reversible loosening of PNNs. Our results indicated that focal cerebral ischemia induces partial depletion of PNNs and that mild hypoperfusion not associated with ischemic injury can induce ultra-structural rearrangements in visually intact meshworks. In line with the activation of neural plasticity under mild stress stimuli, we provide evidence that topological conversion of PNNs can support post stroke neural rewiring.

Introduction

The extracellular matrix (ECM) of the brain is an intricately organized macromolecular network that provides an essential environment for intercellular communication. The establishment and plasticity of local neuronal networks is largely regulated by the ECM [1–3]. Throughout development, the maturation of ECM is related to switching between juvenile and adult types of neural plasticity [4–6]. In adult brain, the relatively diffuse ECM molecules can consolidate into a densely packed layer around a subpopulation of neurons, predominantly the fast-spiking, parvalbumin-containing interneurons [7,8]. These coatings are termed perineuronal nets (PNNs). PNNs are composed by a wide variety of macromolecules originating from various cell types, whose essential backbone is based on hyaluronic acid (hyaluronan, HA) [9], link proteins and chondroitin sulfate proteoglycans (CSPGs) [10]. Enzymatic digestion of CSPGs removes PNNs and re-activates juvenile structural plasticity [6]. In addition to these major components, numerous secreted molecules can be deposited to these scaffolds, including interleukins, growth factors, guidance factors and proteases, which contribute to synapse formation and neural activity regulation [11–14]. PNNs are synthesized on-demand, in an activity-dependent manner [15] and are involved in learning-related neural plasticity [3] via the regulation of AMPA receptor lateral mobility [16]. Serving as polyanionic buffers, these coatings are hypothesized to support the fast spiking properties of neurons by docking the cations in close proximity to the plasma membrane [8,17,18].

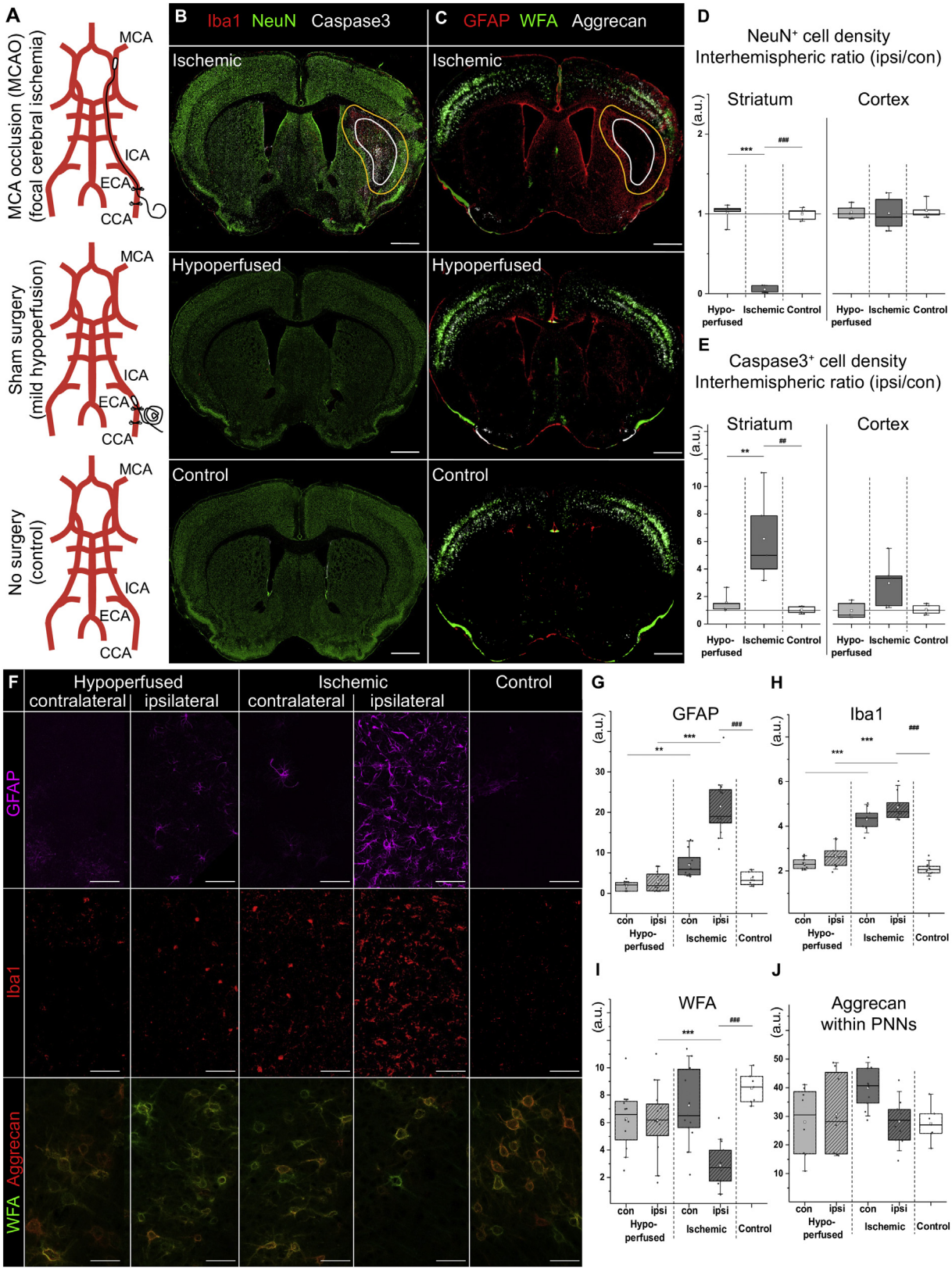
A
MCA occlusion (MCAO) (focal cerebral ischemia)
Sham surgery (mild hypoperfusion)
No surgery (control)
MCA
ICA
ECA
CCA
B Iba1 NeuN Caspase3
C GFAP WFA Aggrecan
Ischemic
Hypoperfused
Control
D
NeuN⁺ cell density
Interhemispheric ratio (ipsi/con)
Striatum
Cortex
(a.u.)
Hypo-perfused
Ischemic
Control
E
Caspase3⁺ cell density
Interhemispheric ratio (ipsi/con)
F
Hypoperfused
contralateral
ipsilateral
Ischemic
contralateral
ipsilateral
Control
GFAP
Iba1
WFA Aggrecan
G
GFAP
H
Iba1
I
WFA
J
Aggrecan within PNNs
con
ipsi
Hypo-perfused
Ischemic
Control

Apparently, because of their crucial role in neural plasticity, PNNs are affected in many neurological diseases, including epilepsy [19], schizophrenia [20], traumatic brain injury [21] and stroke [22]. It has been shown that PNNs can protect neurons against tau pathology [23] and oxidative stress [24,25], which renders these structures a promising target for neuroprotective therapies. In the last decade, ECM-targeting studies focused on the molecular biology of PNN components, and the functional consequences of their depletion. This fruitful research brought us to a new level of understanding of what are the functions of these peculiar structures. However, we still lack knowledge about the structural organization of PNNs. In this study, we developed an approach to quantify the topology of these meshworks, and to understand how brain ischemia modifies them.

Temporary occlusion of middle cerebral artery (MCAO) is widely used as a model of focal cerebral ischemia in rodents [26–28]. Like stroke patients who underwent timely thrombolysis, these animals suffer from focal brain ischemia, followed by reperfusion. Our experimental approach triggers three overlapping phases i) cell death and inflammation, ii) cell proliferation, and iii) tissue remodeling [29]. The first phase of ischemia (roughly the first 7 days) is associated with neuro iflammation, leading to the altered expression of proteoglycans [30,31] and impaired function of the blood-brain barrier (BBB) [32], resulting in the infiltration of plasma proteins, leukocytes and pro-inflammatory interleukins such as tumor necrosis factor-α (TNFα) and interleukin-1β (IL1β) [33]. In addition, the excessive glutamate overstimulates neuronal and glial glutamate receptors and contributes to the activation of phospholipid hydrolysis and disruption of calcium homeostasis, which triggers a devastating cell death by oncosis or apoptosis [34,35]. In the second phase (3–15 days after ischemia), endothelial cells and astrocytes undergo acute proliferation, and the glial scar is formed [36]. Finally, in the remodeling phase (15 days and further), the astrocytic scar and the ischemic core contract, and multiple ECM components are deposited together to build the fibrotic scar [37] inside the ischemic core.

During sub-threshold ischemia, induced by mild hypoperfusion, the brain undergoes hypoxic stress, but no neuronal damage is induced. However, hypoxia triggers a set of metabolic changes, including upregulation of proinflammatory cytokines, heat-shock proteins and growth factors [38], leading to the induction of adaptive neuroprotection. These mechanisms contribute to ischemic tolerance following mild ischemia preconditioning and thus have high clinical relevance [39]. To simulate mild hypoperfusion, we induced a permanent ligation of common carotid artery (CCA), which is usually the sham surgery for our MCAO protocol.

In this study, we explored the reorganization of PNNs in the subacute phase of the cerebral ischemia, when most of the pathological signaling, as well as neuroprotective cascades are triggered. We hypothesized that during this decisive period for neurological recovery, the changes in PNN ultrastructure may be especially pronounced. In addition, we compared the effects of mild hypoperfusion and focal cerebral ischemia on the ultrastructural organization of PNNs. We specifically focused on the cortical PNNs, because no neuronal damage was observed in this region.

Results

The loss of cortical PNNs is associated with persistent gliosis after focal cerebral ischemia

Unilateral focal cerebral ischemia was induced by temporary MCAO. To induce mild hypoperfusion, the left CCA was permanently ligated like in the MCAO surgery (Fig. S1A). Thus, we compared how PNNs are affected by full-scale ischemia and sub-threshold hypoxia. In the subacute phase 10 days after MCAO, the focal lesions were observed in the left (ipsilesional) striatum, surrounded by glial scars (Fig. 1B, C and

Fig. 1. Focal cerebral ischemia, but not mild hypoperfusion, induced cell death, gliosis and loss of cortical PNNs in the ipsilesional hemisphere. (A) The cartoon illustrates the filament placement and ligatures during MCAO and CCA occlusion surgery. In the control condition, no intervention was made. (B, C) The ischemic core (white line) and glial scar (yellow line) is apparent at 10 days after MCAO, but not CCA occlusion surgery. Scale bars, 1 mm. (B) Representative immunolabeling of microglia (Iba1, red), neurons (NeuN, green) and apoptotic cells (activated caspase 3, gray scale) is shown in the coronal sections at bregma level. (C) Representative immunolabeling of reactive astrocytes (GFAP, red) and PNN markers (WFA, green and aggrecan, gray scale) is shown in coronal sections at the bregma level. Note that PNNs are richly expressed in cortical regions, but their presence is less ample in the ipsilesional cortex following MCAO. (D, E) The interhemispheric ratio (ipsilateral/contralateral) quantifications of neuronal ($NeuN^+$) and irreversibly damaged (caspase 3^+) cell densities indicate neuronal loss (D) and cell death (E) in the ipsilesional striatum, but not cortex. (F-J) The loss of cortical PNNs is associated with persistent gliosis at 10 days post ischemia. (F) The panel demonstrates representative immunolabeling of reactive astrocytes (GFAP, magenta), microglia (Iba1, red) and PNN markers (WFA, green and aggrecan, red) in contralesional and ipsilesional cortex of ischemic and hypoperfused animals. Age matched (2 months old) controls are also shown. Scale bars, 50 μm. The labeling intensity quantifications (average pixel intensity) are shown for GFAP (G), Iba1 (H), WFA (I) and aggrecan within WFA-labeled PNNs (J). The box plots show the mean (empty square), the median (line), 25–75% range (borders) and 10–90% range (whiskers). Asterisks indicate significant differences with the hypoperfusion, hatches with the control condition, based on two-way repeated ANOVA ($^{**,\#\#}p < 0.01$; $^{***,\#\#\#}p < 0.001$).

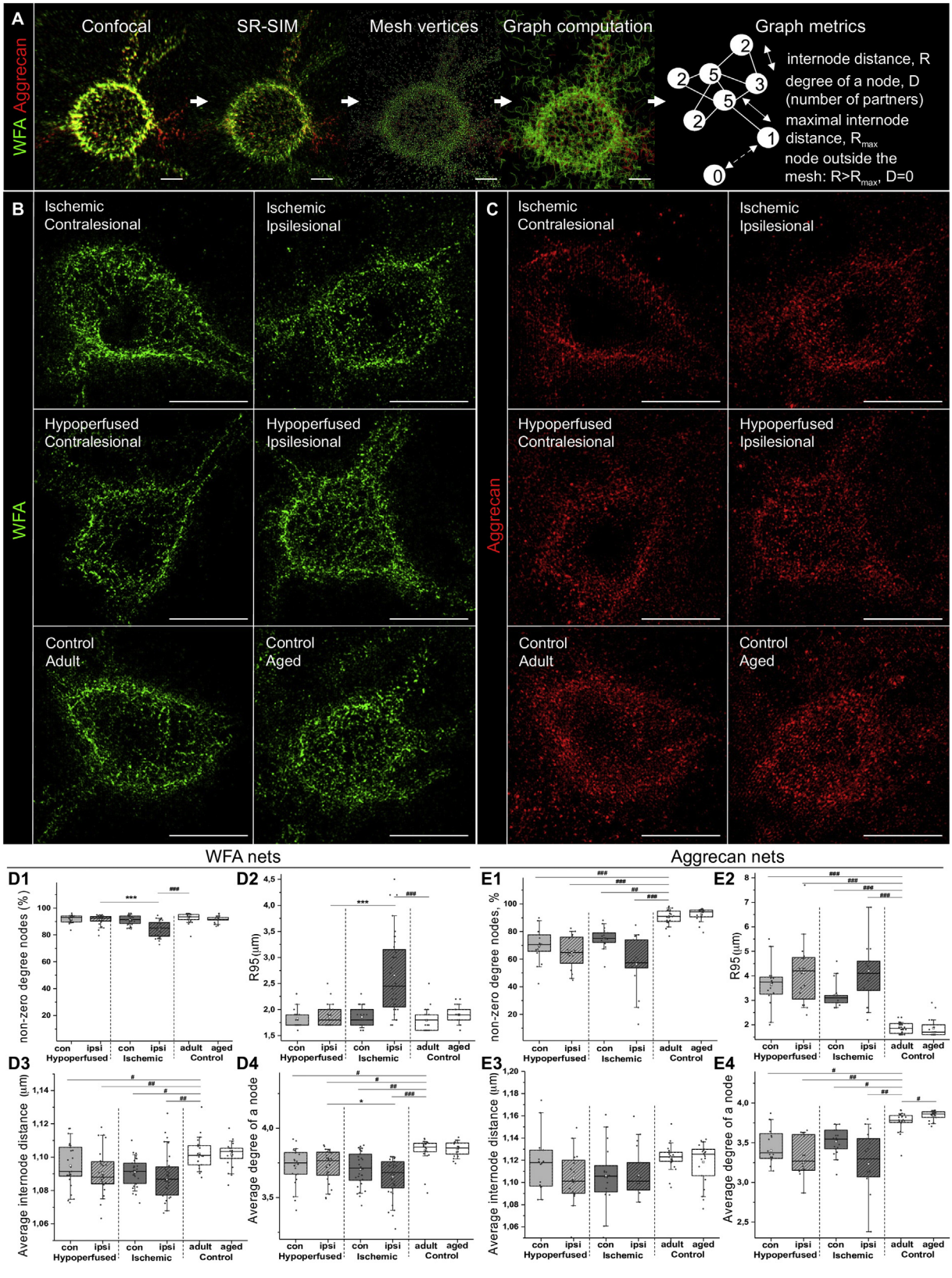
A
WFA Aggrecan
Confocal
SR-SIM
Mesh vertices
Graph computation
Graph metrics
internode distance, R
degree of a node, D
(number of partners)
maximal internode
distance, Rmax
node outside the
mesh: R>Rmax, D=0
B
C
WFA
Aggrecan
Ischemic
Contralesional
Ischemic
Ipsilesional
Hypoperfused
Contralesional
Hypoperfused
Ipsilesional
Control
Adult
Control
Aged
WFA nets
Aggrecan nets
D1
D2
D3
D4
E1
E2
E3
E4
non-zero degree nodes (%)
R95 (µm)
Average internode distance (µm)
Average degree of a node
con
ipsi
con
ipsi
adult
aged
Hypoperfused
Ischemic
Control

Fig. S1). The interhemispheric ratios (ipsilesional/contralesional) indicated the reduction of neurons (NeuN positive) and appearance of irreversibly injured (active caspase-3 positive) cells in the ipsilesional striatum, but not cortex (Fig. 1D, E). Mild hypoperfusion following CCA occlusion did not induce neuronal death neither in cortex, nor striatum. Wherein the cortex was not part of ischemic lesion, reactive gliosis was observed in this region following MCAO, as indicated by the upregulation of astrocytic marker GFAP and microglial marker Iba1 (Fig. 1F, G, H and Fig. S1). To a lesser degree, reactive gliosis was also observed in the contralesional somatosensory cortex following MCAO. In the CCA occlusion group, mild hypoperfusion did not induce significant elevation of GFAP and Iba1 signals, compared with control animals. Conjointly with reactive gliosis, MCAO induced the partial loss of PNN labeling (Fig. 1F, I and Fig. S2), as indicated by the fluorescence intensity quantification of *Wisteria floribunda* lectin (WFA). WFA binds to the disaccharide LacdiNAc chondroitin sulfate chains of CSPGs within the proteoglycans of PNNs [40,41] and is therefore used as a classical marker of these structures. Although hypoperfusion also moderately decreased the intensity of WFA, the evident loss of PNNs was observed only in the ipsilesional cortex following MCAO and was not associated with neuronal cell death (Fig. 1C, F, I). Interestingly, within the remaining WFA-labeled nets, the fluorescence intensity of aggrecan core protein (one of the key CSPGs of PNNs) was not notably different across groups (Fig. 1C, F, J and Fig. S2). The analysis of total aggrecan expression in the perilesional cortex via immunoblotting did not reveal a significant difference between the ischemic and mild hypoperfusion groups (Fig. S3).

Graph construction reveals the 3D topology of PNNs

To analyze the PNN ultrastructure, we elaborated a quantitative approach combining 3D superresolution imaging and mathematical reconstruction, which revealed the topology of these meshworks (Fig. 2A and Supplementary Video 1). By using the glycan-binding marker WFA and anti-aggrecan specific antibody, we visualized the distribution of both side chains and the core protein of PNN-composing CSPGs. Because PNNs are known to evolve throughout development [42], both adult (2 months) and aged (>15 months) controls were included. We observed no remarkable differences between the adult and aged controls, suggesting the maturity of PNNs in 2 month-old mice.

Because of the high complexity and density of PNNs [10], it is not possible to resolve their 3D organization by means of conventional microscopy. In our experiments, structured illumination microscopy (SIM) provided the reliable and reproducible resolution of at least 200 nm in lateral and 400 nm in axial directions in the highly scattering brain slices at all depths of the sample (Fig. S4). Following SIM imaging, the vertices of WFA or aggrecan labeled nets were localized as fluorescence intensity centers, in accordance with previous studies [43]. The vertices of 3D meshes were assigned as graph nodes, and the net-like structure of a PNN was then reconstructed using the custom developed graph computation algorithm. From the resulting graphs, the four topological metrics were derived for further statistical analysis: i) percentage of nodes with non-zero degree; ii) maximal internode distance, at which 95% of the nodes have non-zero degree (this metric will be further abbreviated as R95); iii) average internode distance; iv) average degree of a node.

Both focal cerebral ischemia and mild hypoperfusion alter the ultrastructural organization of cortical PNNs

Ultrastructural analysis was conducted for those PNN meshes, which were visually intact and expressed a pronounced labeling of both WFA and aggrecan (Fig. 2B, C). The PNN topology was separately analyzed in the ipsilesional or contralesional cortex after focal ischemia, induced by MCAO or mild hypoperfusion following CCA occlusion. In the control group a comparable number of nets was analyzed in the left and right cortex. Two complementary metrics were used as a measure of mesh integrity: percentage

Fig. 2. The ultrastructure of cortical PNNs is altered by both focal cerebral ischemia and mild hypoperfusion. Graph based reconstruction of a PNN topology and key metrics are shown in (A). Scale bar, 5 μm. The major components of PNNs were labeled with WFA lectin (green), and the antibody against aggrecan core protein (red). Maximum intensity projections following confocal and superresolution structured illumination microscopy (SR-SIM) are shown. The vertices of WFA and aggrecan-labeled meshes were identified as fluorescence intensity centers. The undirected graph was computed using a find-the-neighbor algorithm, reconstituting the PNN structure. For the 3D reconstruction of this PNN, see Supplementary Video 1. (B, C) The panels demonstrate representative maximum intensity projections of single PNNs labeled with WFA lectin (green) and anti-aggrecan core protein (red) in contralesional and ipsilesional cortex of ischemic and hypoxic animals. Adult (2 months old) and aged (>15 months old) controls are also shown. Scale bars, 5 μm. The topology of WFA-labeled nets (D1–D4) and aggrecan-labeled nets (E1–E4) was quantified using the four metrics (see main text): percentage of non-zero degrees (D1, E1), average R95 (D2, E2), average internode distance (D3, E3) and average degree of a node (D4, E4). The box plots show the mean (empty square), the median (line), 25–75% range (borders) and 10–90% range (whiskers). Asterisks indicate significant differences with the hypoperfusion, hatches – with the adult control condition, based on two-way repeated ANOVA ($^{**,\#\#}p < 0.01$; $^{***,\#\#\#}p < 0.001$).

of nodes with non-zero degree and the R95 metric. The lower proportion of non-zero degree nodes and higher R95 values correspond to more diffuse meshworks. In the ipsilesional cortex of ischemic animals, WFA nets were significantly more diffuse compared to hypoperfused and control animals, indicating partial dissociation (Fig. 2D1, D2). We did not observe a difference in the integrity of aggrecan-labeled meshes between ipsilesional ischemic and hypoperfused cortices (Fig. 2E1, E2), but in both groups the nets were more scattered than the control ones. Average internode distance and average degree in WFA labeled nets were significantly decreased in both hemispheres of both ischemic and hypoperfused animals (Fig. 2D3, D4). Notably, in the ischemic ipsilesional cortex, only the degree, but not the internode distance of WFA meshes was more strongly reduced, compared to mild hypoperfusion. In the meantime, the average internode distance of aggrecan labeled nets was affected by neither mild hypoperfusion, nor focal cerebral ischemia, while the degree of a node was similarly decreased in both groups on both sides (Fig. 2E1, E2). The exact mean values and standard deviations of all topological metrics are provided in Table S1.

Discussion

The ultrastructural organization of PNNs remained unresolved mainly due to their complex and condensed constitution. To our knowledge the characterization of their net-like morphology has originally been based on qualitative assessment, until recently the first attempt was made to quantitatively analyze the geometry of PNNs [43]. This latter study has proven that the pattern of WFA labeling, which is typically used to identify PNNs, indeed corresponds to a polygonal mesh, with the polygon vertices located in the local intensity maxima. However, the authors did not explore the 3D structure of perineuronal coatings. Also, it was not clear, whether the geometry of PNNs is linked to neuropathology.

Today, the advances in light microscopy techniques complement the benefits of immunofluorescent labeling with unprecedented resolution of imaging. In this work, the combination of SR-SIM and automated data processing algorithms enabled us to provide the first estimation of PNN topology. We focused on the ultrastructural alterations of these meshes in response to focal cerebral ischemia mainly because of their pivotal role in regulating neural plasticity [13,44–46]. Several components of PNNs, including CSPGs, are known to restrict axonal outgrowth, and their removal can facilitate post stroke recovery [4]. However, the reactive astrocytes of the posttraumatic glial scar release a set of CSPGs that aid axon regeneration [47,48]. The loss of PNNs results in altered synaptic plasticity [49,50], leads to epileptiform activity [17] and is associated with psychosis [51]. Importantly, PNNs can protect neurons against several types of neuropathology [23,25]. After photothrombosis, the reduction of PNNs in the perilesional area is not associated with neuronal death [52]. In addition, the perineuronal coatings are partially restored in the late recovery phase [52], suggesting that the post-stroke depletion of PNNs is not a result of cell death but a process to facilitate local neural plasticity. This evidence suggests that the subtle modulation, but not crude depletion of extracellular matrix may help to improve functional recovery after brain injury. But before we can seek a way to do so, we need to understand how PNNs are constructed and what changes they undergo after brain injury.

Rodent models of focal cerebral ischemia provide a valuable tool to investigate stroke mechanisms and approaches for the post-stroke restorative therapies [28]. In mice, temporary MCAO is widely used to investigate both acute and chronic phases of stroke [53]. The permanent ligation of CCA, which is a part of the classical MCAO protocol developed by Koizumi [54], is also used as a separate model [55] to study subthreshold hypoperfusion that does not result in structural brain injury, but causes mild hypoxia [56]. In this work, we performed Koizumi's MCAO to induce ischemia, and permanent CCA ligation to induce mild hypoperfusion. In the control group, the brain-supplying vasculature was left intact.

In accordance with a previous study [22], we found a significant reduction of PNNs in the perilesional cortex after MCAO, which was associated with the highest level of glia reactivity.

At the ultrastructural level, the topology of WFA and aggrecan labeled meshes were differently affected. While the WFA meshes became more diffuse only upon ischemia, the topology of aggrecan nets was affected already by mild hypoperfusion, as indicated by R95 metric. However, the internode distance of aggrecan meshes was not affected, contrary to WFA. The average degree of a node in both networks was significantly reduced upon both hypoperfusion and ischemia, but this metric was not further affected by MCAO in aggrecan nets. In addition, both general expression of aggrecan (a core CSPG of PNNs) and its content in the intact meshes were not substantially affected after ischemia. This observation hints at the potential role of aggrecan for PNN stability. Together, these results indicate higher stability of aggrecan topology. Hypothetically, hypoxia can induce initial rearrangement of a PNN backbone during both ischemia and hypoperfusion. This carcass appears to be more resistant to the increasing severity of injury, while the stability of glycan side chains can be further compromised alongside with the increased level of neuroinflammatory responses, in accordance with previous studies [31].

Taken in view the severity of brain injury after MCAO surgery, it is surprising that the observed ultrastructural

alterations of cortical PNNs in mild hypoperfusion are so similar to focal cerebral ischemia. Hypothetically, the impairment of blood flow in both cases can induce microglia proliferation [55] and peripheral immune cell infiltration [57], leading to the elevated production of long-range signaling factors like transforming growth factor-β (TGFβ), which can induce PNN decomposition [58]. And although the expansion of the ischemic core is localized by the astrocytic scar at this stage [59], interleukins may diffuse into distant brain areas [60]. Since the general loss of WFA labeling is evidently stronger in the ipsilesional cortex after MCAO, compared to contralateral cortex or hypoperfusion, deconstruction of PNNs may depend on a pro-inflammatory signal gradient.

A close look at the topology metrics change reveals another very intriguing observation. For both WFA and aggrecan labeled meshworks, the degree of a node may drop (compare ipsilesional hypoperfusion and ischemia) while internode distance remains unaffected. This observation points to the fact that the ultrastructural changes in PNNs after ischemia are not simply a dissociation of nodes from the net. We propose that the vertices of the meshwork may stay together, while the pattern of their interlinking is altered. Fig. 3 offers a graphical explanation of this hypothesis. Based on our results we suggest, that prior to dissociation under severe injury, the regular meshwork will undergo a potentially reversible transition to a loosened state. Because the internode boundaries length remains unaltered, or can even become slightly stretched, we propose to call this state as a tension regime.

The existence of such intermediate quasi stable states is known for many biological systems [61]. As a rule, falling into these states is reversible. With regard to the balance between neuroplasticity and neuroprotection after stroke, our explanation offers a new understanding of ECM as a dynamic system, which should be deeper investigated with regard to neuropathological mechanisms. Theoretically, the topological tension regime of PNN ultrastructure may facilitate local rewiring after stroke. Because PNN-coated neurons are central for neural synchronization, enhancing the plasticity of these cells can strongly influence the activity of local neural networks [62–64]. We hypothesize that in both ischemic and hypoperfused conditions, the tension state of a PNN topology may be reverted back to the original organization. At this point, the timeline of such reversal is not clear and needs further investigation. Interestingly, the slow recovery of several PNN components was observed after cortical photothrombotic stroke in rats [52].

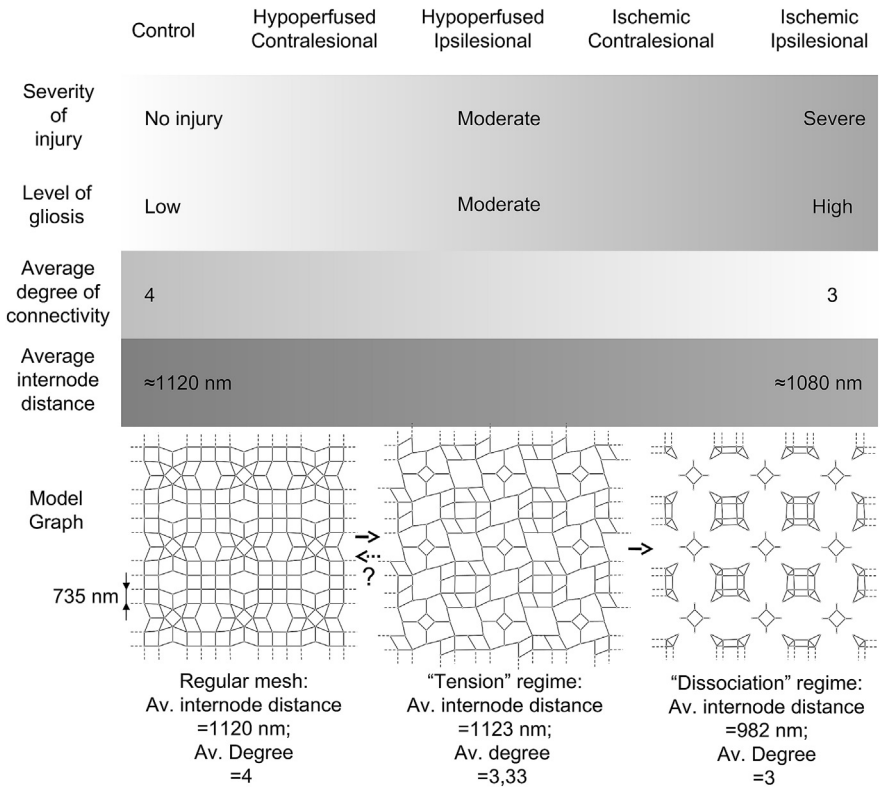

Fig. 3. The stepwise rearrangement of PNN topology is linked to the severity of ischemia and gliosis. Based on our results, the average degree of a node may decrease while the average internode distance remains unaltered. This observation points to the existence of an intermediate "tension" regime before PNNs dissociate. The hypothetical two-step topological conversion within PNNs is illustrated using a model graph.

Our hypothesis is in agreement with the experimentally proven facilitation of neural plasticity following subthreshold hypoperfusion, which is extensively explored in the scope of ischemic preconditioning. The induction of mild hypoperfusion can render brain tissue tolerant to subsequent lethal injuries [39], and some methodologies of hypoxic preconditioning, like hypothermia, are already clinically approved [65,66]. The induction of ischemic tolerance is associated with facilitated synaptic potentiation [67] and results in improved spatial cognition after sub-threshold hypoxia in mice [68]. This enhancement of synaptic plasticity potentially arises from brain-derived neurotrophic factor (BDNF) mediated activation of PKCε [69]. In addition, neural plasticity can be enhanced by the moderate neuroinflammatory response and early release of TNFα, TGFβ and IL1β [38,70,71] following ischemic preconditioning.

To date, it is not known whether the modification of the neural extracellular matrix plays a role in the development of ischemic tolerance. However, our data indicates that structural reorganization of PNNs is an important response to mild hypoperfusion events that potentially triggers neuroplasticity.

Experimental procedures

Legal issues, animal housing, randomization and blinding

Experiments were performed with local government approval (Bezirksregierung Düsseldorf) in accordance to E.U. guidelines (Directive 2010/63/EU) for the care and use of laboratory animals and ARRIVE guidelines. The experimenter performing the histochemical studies (E.D.) was fully blinded at all stages of the study by another researcher (D.M.-C.) who performed animal surgeries. Animals were kept in a regular inverse 12 h:12 h light/dark cycle in groups of 5 animals/cage.

Animal groups, induction of cerebral ischemia and mild hypoperfusion

Male C57/Bl6 wildtype mice (at the age of 2 months) were assigned into three groups: focal cerebral ischemia (MCAO surgery), mild hypoperfusion (CCA occlusion surgery) and age-matched control. In addition, an elderly control group (age > 15 months) was formed. Each group included 5 animals. MCAO was performed using an intraluminal filament technique. Animals were anesthetized with 1.5% v/v isoflurane (30% v/v O_2, remainder N_2O) and 150 µl of buprenorphine was injected subcutaneously. An incision was made in the neck that exposed the left CCA. The lower part of the CCA was permanently ligated. A fine incision into the CCA was made, through which a silicon-coated nylon monofilament was introduced and advanced through the internal carotid artery, until it blocked the bifurcation of the middle cerebral artery (MCA). Laser Doppler flow (LDF) was measured above the MCA territory to control blood supply cessation. After 30 min of MCAO, reperfusion was induced by removing the filament, while the CCA remained permanently blocked. The recovery of blood supply was controlled by LDF recording. In the hypoperfusion group, mild hypoxia was induced by the permanent ligation of the CCA. In control groups, no surgical intervention was made. Postsurgical care was provided by daily administration of 250 µl of a cocktail containing 2% carprofen and 5% glucose in Ringer's solution for seven days.

Immunohistochemistry

At 10 days post-surgery, animals were anesthetized with 100 µl of 2% w/v ketamine-10% w/v xylazin mixture (1:3) and perfused with 20 ml of cooled saline, followed by 20 ml of cooled 4% w/v paraformaldehyde (PFA) in 0.1 M Tris buffer saline (TBS), pH 8.0. Then, the brains were removed and immersed in 4% w/v PFA in TBS overnight at 4 °C. Tissue was cryoprotected by gradient incubation in 15%–30% w/v sucrose for 2 days and frozen at –80 °C. Coronal sections (30 µm thick) were obtained at the bregma level using a Leica CM1950 cryostat, rinsed three times with 0.1 M phosphate buffer saline (PBS) and immersed in PBS containing 0.3% w/v Triton X-100 (PBS-T) and 10% v/v normal donkey serum for 1 h at room temperature. Sections were incubated overnight at 4 °C in PBS containing 0.1% w/v Triton X-100 and primary antibodies mixture. To visualize neurons, microglia and apoptotic cells, we used monoclonal mouse anti-NeuN (1:500; MAB377; Merck Millipore), polyclonal goat anti-ionized calcium binding adaptor protein (Iba-1) (1:300; ab5076; Abcam) and polyclonal rabbit anti-activated caspase 3 (1:300; 9662; Cell Signalling). For labelling of astrocytes and PNN components, we applied monoclonal mouse anti-glial acidic protein (GFAP) (1:500; 3670 s; Cell Signalling), polyclonal rabbit anti-aggrecan (1:500, AB1031; Merck Millipore) and biotinylated *Wisteria floribunda* lectin (WFA) (1:100; L1516; Sigma). Primary antibodies were detected with appropriate secondary antibody, conjugated to Alexa Fluor-488, Alexa Fluor-594 or Alexa Fluor-647. Lastly, the bound antibodies were stabilized by incubating the sections in 2% w/v PFA for 20 min at room temperature.

Neuronal and irreversibly damaged cell density analysis

The entire brain sections, labeled for NeuN and activated caspase 3 antigens, were scanned with the Olympus VS120 Virtual Slide Microscope (20× Plan Apochromat objective, NA 0.75, pixel size 0.33 µm). Imaging parameters were manually optimized and were not changed across the experiments. The

obtained images were exported to ImageJ and the cell density was analyzed in the entire cortex or striatum of each hemisphere. The analysis was performed using a custom written user-independent script, based on standard ImageJ functions. The results were expressed as interhemispheric ratios (ipsilateral/contralateral).

Intensity based analysis of glial and PNN markers

To provide a reliable quantification of GFAP, Iba1, aggrecan and WFA labeling intensity, single plane 425.1 × 425.1 μm micrographs were obtained in the cortical regions using the Carl Zeiss LSM 710 confocal microscope (20× Plan Apochromat objective, NA 0.8, pixel size 0.21 μm). Four micrographs obtained from two adjacent brain sections were investigated for each animal in the ipsilesional and contralesional cortex. Images were exported to ImageJ and average pixel intensity of GFAP, Iba1 and WFA labelling was analyzed using an automated routine. To quantify the content of aggrecan within PNNs, the average pixel intensity of aggrecan labelling was analyzed inside WFA-labeled regions of interest using a custom written user-independent script, based on standard ImageJ functions.

Reconstruction and analysis of PNN topology

Superresolution structured illumination microscopy (SR-SIM) of PNNs was performed using the Carl Zeiss Elyra PS.1 SR-SIM microscope. For each PNN-coated cell, an individual 83.13 × 83.13 × 8.18 μm z-stack was obtained (100× alpha Plan-Apochromat objective, NA 1.46, voxel size 65x65x101 nm). The complete list of imaging settings is provided in the Supplementary Table 2. Only those PNNs which expressed a profound labelling with the WFA lectin and anti-aggrecan antibody were analyzed with SR-SIM. For each animal, 8 individual PNNs were analyzed in the ipsilesional and contralesional cortex from two adjacent brain sections. The output super-resolution images were computed using the automatic processing mode using the Zen Black program from Zeiss. The resulting 3D stacks were imported into the IMARIS program, and the mesh vertices of PNNs were localized using the semi-automated “dots” pipeline. Vertex positions were imported into MatLab and the 3D PNN meshwork was reconstructed in a form of undirected graph using a custom developed algorithm, provided as a supplementary file. In brief, a mesh vertex was connected to its neighbor, if the linear distance between them was smaller than the maximum distance (a user defined parameter), but bigger than the minimum distance (derived from the resolution of imaging), and the connection was not yet formed. By default, maximum distance was 1,5 μm, based on the diameter of net facets. Graph computation was performed independently for WFA and aggrecan labeled nets, and four topological metrics were derived: i) percentage of nodes with non-zero degree; ii) maximal internode distance, at which 95% of the nodes have non-zero degree (this metric will be further abbreviated as R95); iii) average internode distance; iv) average degree of a node (number of neighboring nodes it connects).

Statistical analysis

All quantitative data was presented as box plots indicating the mean (empty square), the median (line), 25–75% range (borders) and 10–90% range (whiskers) of data distribution. For all datasets, the normality of distribution was analyzed using the Kolmogorov-Smirnov test. The differences between populations were evaluated using two-way repeated measurement analysis of variance (ANOVA). For multiple comparisons, Bonferroni correction was applied.

Supplementary data to this article can be found online at https://doi.org/10.1016/j.matbio.2018.08.001.

Acknowledgements

The authors sincerely appreciate the grant support by the German Research Council (He 3173/3-1 and He 3173/11-1 to D.M.H., SFB 642 TP A24 and Fa 159/22-1 to A.F.). E.D. was supported by a training grant of the International Graduate School of Neuroscience (IGSN), Ruhr-University Bochum during part of this work. For the maintenance of equipment, pivotal advice and critical discussion of SR-SIM methodology, the authors are especially thankful to the IMCES (imaging center Essen) staff. The authors thank Dr. Happel (STED Facility, RUBION, Ruhr-University) for helpful discussions.

Author contributions

E.D., D.M.H. and A.F. designed and planned the study. A.F. and D.M.H. provided supervision and project administration, A.F., C.K. and D.M.H. funding. D.M.-C. performed animal surgeries, Western Blot experiments and analysis. E.D. carried out immunocytochemistry, imaging and image analysis. E.D. and D.M.H. drafted the manuscript. All authors discussed the data and contributed to the final version of the manuscript.

Declaration of interest

The authors have no competing interests related to this work.

Received 30 April 2018;
Received in revised form 2 August 2018;
Accepted 2 August 2018
Available online 6 August 2018

Keywords:
Hypoxia;
Ischemic stroke;
Middle cerebral artery occlusion;
Neural plasticity;
Structured illumination microscopy;
Superresolution microscopy;
Extracellular matrix

†Equal contribution.

References

[1] A. Dityatev, M. Schachner, P. Sonderegger, The dual role of the extracellular matrix in synaptic plasticity and homeostasis, Nat. Rev. Neurosci. 11 (11) (2010) 735–746.
[2] L.E. Clarke, B.A. Barres, Emerging roles of astrocytes in neural circuit development, Nat. Rev. Neurosci. 14 (5) (2013) 311–321.
[3] R. Frischknecht, E.D. Gundelfinger, M.R.K.A.C. Sala, The Brain's Extracellular Matrix and Its Role in Synaptic Plasticity, Advances in Experimental Medicine and Biology, Springer-Verlag/Wien 2012, pp. 153–171.
[4] D. Bavelier, D.M. Levi, R.W. Li, Y. Dan, T.K. Hensch, Removing brakes on adult brain plasticity: from molecular to behavioral interventions, J. Neurosci. 30 (45) (2010) 14964–14971.
[5] E.D. Gundelfinger, R. Frischknecht, D. Choquet, M. Heine, Converting juvenile into adult plasticity: a role for the brain's extracellular matrix, Eur. J. Neurosci. 31 (12) (2010) 2156–2165.
[6] T. Pizzorusso, P. Medini, N. Berardi, S. Chierzi, J.W. Fawcett, L. Maffei, Reactivation of ocular dominance plasticity in the adult visual cortex, Science 298 (5596) (2002) 1248–1251.
[7] W. Härtig, K. Brauer, G. Bruckner, Wisteria floribunda agglutinin-labelled nets surround parvalbumin-containing neurons, Neuroreport 3 (10) (1992) 869–872.
[8] W. Härtig, A. Derouiche, K. Welt, K. Brauer, J. Grosche, M. Mäder, A. Reichenbach, G. Brückner, Cortical neurons immunoreactive for the potassium channel Kv3.1b subunit are predominantly surrounded by perineuronal nets presumed as a buffering system for cations, Brain Res. 842 (1) (1999) 15–29.
[9] W. Su, S. Matsumoto, B. Sorg, L.S. Sherman, Distinct roles for hyaluronan in neural stem cell niches and perineuronal nets, Matrix Biol. (2018) https://doi.org/10.1016/j.matbio.2018.01.022.
[10] D. Carulli, K.E. Rhodes, D.J. Brown, T.P. Bonnert, S.J. Pollack, K. Oliver, P. Strata, J.W. Fawcett, Composition of perineuronal nets in the adult rat cerebellum and the cellular origin of their components, J. Comp. Neurol. 494 (4) (2006) 559–577.
[11] M. Beurdeley, J. Spatazza, H.H. Lee, S. Sugiyama, C. Bernard, A.A. Di Nardo, T.K. Hensch, A. Prochiantz, Otx2 binding to perineuronal nets persistently regulates plasticity in the mature visual cortex, J. Neurosci. 32 (27) (2012) 9429–9437.
[12] D. Carulli, S. Foscarin, A. Faralli, E. Pajaj, F. Rossi, Modulation of semaphorin3A in perineuronal nets during structural plasticity in the adult cerebellum, Mol. Cell. Neurosci. 57 (2013) 10–22.
[13] E. Dzyubenko, C. Gottschling, A. Faissner, Neuron-glia interactions in neural plasticity: contributions of neural extracellular matrix and perineuronal nets, Neural Plast. 2016 (2016) 1–14.
[14] J. Wlodarczyk, I. Mukhina, L. Kaczmarek, A. Dityatev, Extracellular matrix molecules, their receptors, and secreted proteases in synaptic plasticity, Dev. Neurobiol. 71 (11) (2011) 1040–1053.
[15] A. Dityatev, G. Bruckner, G. Dityateva, J. Grosche, R. Kleene, M. Schachner, Activity-dependent formation and functions of chondroitin sulfate-rich extracellular matrix of perineuronal nets, Dev. Neurobiol. 67 (5) (2007) 570–588.
[16] R. Frischknecht, M. Heine, D. Perrais, C.I. Seidenbecher, D. Choquet, E.D. Gundelfinger, Brain extracellular matrix affects AMPA receptor lateral mobility and short-term synaptic plasticity, Nat. Neurosci. 12 (7) (2009) 897–904.
[17] A.M. Arranz, K.L. Perkins, F. Irie, D.P. Lewis, J. Hrabe, F. Xiao, N. Itano, K. Kimata, S. Hrabetova, Y. Yamaguchi, Hyaluronan deficiency due to Has3 knock-out causes altered neuronal activity and seizures via reduction in brain extracellular space, J. Neurosci. 34 (18) (2014) 6164–6176.
[18] E. Sykova, C. Nicholson, Diffusion in brain extracellular space, Physiol. Rev. 88 (4) (2008) 1277–1340.
[19] P.A. McRae, E. Baranov, S.L. Rogers, B.E. Porter, Persistent decrease in multiple components of the perineuronal net following status epilepticus, Eur. J. Neurosci. 36 (11) (2012) 3471–3482.
[20] S.A. Mauney, K.M. Athanas, H. Pantazopoulos, N. Shaskan, E. Passeri, S. Berretta, T.U. Woo, Developmental pattern of perineuronal nets in the human prefrontal cortex and their deficit in schizophrenia, Biol. Psychiatry 74 (6) (2013) 427–435.
[21] T.H. Hsieh, H.H.C. Lee, M.Q. Hameed, A. Pascual-Leone, T. K. Hensch, A. Rotenberg, Trajectory of parvalbumin cell impairment and loss of cortical inhibition in traumatic brain injury, Cereb. Cortex 27 (12) (2017) 5509–5524 (New York, N.Y.: 1991).
[22] W. Hartig, B. Mages, S. Aleithe, B. Nitzsche, S. Altmann, H. Barthel, M. Krueger, D. Michalski, Damaged neocortical perineuronal nets due to experimental focal cerebral ischemia in mice, rats and sheep, Front. Integr. Neurosci. 11 (2017) 15.
[23] M. Morawski, G. Bruckner, C. Jager, G. Seeger, T. Arendt, Neurons associated with aggrecan-based perineuronal nets are protected against tau pathology in subcortical regions in Alzheimer's disease, Neuroscience 169 (3) (2010) 1347–1363.
[24] M. Morawski, M.K. Bruckner, P. Riederer, G. Bruckner, T. Arendt, Perineuronal nets potentially protect against oxidative stress, Exp. Neurol. 188 (2) (2004) 309–315.
[25] J.-H. Cabungcal, P. Steullet, H. Morishita, R. Kraftsik, M. Cuenod, T.K. Hensch, K.Q. Do, Perineuronal nets protect fast-spiking interneurons against oxidative stress, Proc. Natl. Acad. Sci. 110 (22) (2013) 9130–9135.
[26] S.A. Liddelow, K.A. Guttenplan, L.E. Clarke, F.C. Bennett, C. J. Bohlen, L. Schirmer, M.L. Bennett, A.E. Münch, W.-S. Chung, T.C. Peterson, D.K. Wilton, A. Frouin, B.A. Napier, N.

Panicker, M. Kumar, M.S. Buckwalter, D.H. Rowitch, V.L. Dawson, T.M. Dawson, B. Stevens, B.A. Barres, Neurotoxic reactive astrocytes are induced by activated microglia, Nature 541 (7638) (2017) 481–487.
[27] Y. Wang, R. An, G.K. Umanah, H. Park, K. Nambiar, S.M. Eacker, B. Kim, L. Bao, M.M. Harraz, C. Chang, R. Chen, J.E. Wang, T.-I. Kam, J.S. Jeong, Z. Xie, S. Neifert, J. Qian, S.A. Andrabi, S. Blackshaw, H. Zhu, H. Song, G.-L. Ming, V.L. Dawson, T.M. Dawson, A nuclease that mediates cell death induced by DNA damage and poly(ADP-ribose) polymerase-1, Science 354 (6308) (2016) (New York, N.Y.). (aad6872).
[28] P. Venkat, Y. Shen, M. Chopp, J. Chen, Cell-based and pharmacological neurorestorative therapies for ischemic stroke, Neuropharmacology 134 (Pt B) (2018) 310–322.
[29] J.E. Burda, M.V. Sofroniew, Reactive gliosis and the multicellular response to CNS damage and disease, Neuron 81 (2) (2014) 229–248.
[30] F. Heindryckx, J.P. Li, Role of proteoglycans in neuro-inflammation and central nervous system fibrosis, Matrix Biol. 68-69 (2018) 589–601.
[31] E.L. Stephenson, V.W. Yong, Pro-inflammatory roles of chondroitin sulfate proteoglycans in disorders of the central nervous system, Matrix Biol. 71–72 (2018) 432–442.
[32] M. Krueger, I. Bechmann, K. Immig, A. Reichenbach, W. Hartig, D. Michalski, Blood-brain barrier breakdown involves four distinct stages of vascular damage in various models of experimental focal cerebral ischemia, J. Cereb. Blood Flow Metab. 35 (2) (2015) 292–303.
[33] A. Liesz, X. Hu, C. Kleinschnitz, H. Offner, Functional role of regulatory lymphocytes in stroke: facts and controversies, Stroke 46 (5) (2015) 1422–1430.
[34] G. Kroemer, L. Galluzzi, P. Vandenabeele, J. Abrams, E.S. Alnemri, E.H. Baehrecke, M.V. Blagosklonny, W.S. El-Deiry, P. Golstein, D.R. Green, M. Hengartner, R.A. Knight, S. Kumar, S.A. Lipton, W. Malorni, G. Nunez, M.E. Peter, J. Tschopp, J. Yuan, M. Piacentini, B. Zhivotovsky, G. Melino, Nomenclature Committee on Cell, Classification of cell death: recommendations of the Nomenclature Committee on Cell Death 2009, Cell Death Differ. 16 (1) (2009) 3–11.
[35] T.W. Lai, S. Zhang, Y.T. Wang, Excitotoxicity and stroke: identifying novel targets for neuroprotection, Prog. Neurobiol. 115 (2014) 157–188.
[36] S.D. Magaki, C.K. Williams, H.V. Vinters, Glial function (and dysfunction) in the normal & ischemic brain, Neuropharmacology 134 (Pt B) (2018) 218–225.
[37] D.O. Dias, C. Goritz, Fibrotic scarring following lesions to the central nervous system, Matrix Biol. 68-69 (2018) 561–570.
[38] U. Dirnagl, R.P. Simon, J.M. Hallenbeck, Ischemic tolerance and endogenous neuroprotection, Trends Neurosci. 26 (5) (2003) 248–254.
[39] S. Li, A. Hafeez, F. Noorulla, X. Geng, G. Shao, C. Ren, G. Lu, H. Zhao, Y. Ding, X. Ji, Preconditioning in neuroprotection: from hypoxia to ischemia, Prog. Neurobiol. 157 (2017) 79–91.
[40] S. Miyata, S. Nadanaka, M. Igarashi, H. Kitagawa, Structural variation of chondroitin sulfate chains contributes to the molecular heterogeneity of perineuronal nets, Front. Integr. Neurosci. 12 (2018) 3.
[41] O. Haji-Ghassemi, M. Gilbert, J. Spence, M.J. Schur, M.J. Parker, M.L. Jenkins, J.E. Burke, H. van Faassen, N.M. Young, S.V. Evans, Molecular basis for recognition of the cancer glycobiomarker, LacdiNAc (GalNAc[beta1 → 4] GlcNAc), by Wisteria floribunda Agglutinin, J. Biol. Chem. 291 (46) (2016) 24085–24095.
[42] I. Song, A. Dityatev, Crosstalk between glia, extracellular matrix and neurons, Brain Res. Bull. 136 (2018) 101–108.
[43] N. Arnst, S. Kuznetsova, N. Lipachev, N. Shaikhutdinov, A. Melnikova, M. Mavlikeev, P. Uvarov, T.V. Baltina, H. Rauvala, Y.N. Osin, A.P. Kiyasov, M. Paveliev, Spatial patterns and cell surface clusters in perineuronal nets, Brain Res. 1648 (Pt A) (2016) 214–223.
[44] A. Bikbaev, R. Frischknecht, M. Heine, Brain extracellular matrix retains connectivity in neuronal networks, Sci. Rep. 5 (2015) 14527.
[45] B.A. Sorg, S. Berretta, J.M. Blacktop, J.W. Fawcett, H. Kitagawa, J.C. Kwok, M. Miquel, Casting a wide net: role of perineuronal nets in neural plasticity, J. Neurosci. 36 (45) (2016) 11459–11468.
[46] S. Miyata, H. Kitagawa, Formation and remodeling of the brain extracellular matrix in neural plasticity: roles of chondroitin sulfate and hyaluronan, Biochim. Biophys. Acta 1861 (10) (2017) 2420–2434.
[47] M.A. Anderson, J.E. Burda, Y. Ren, Y. Ao, T.M. O'Shea, R. Kawaguchi, G. Coppola, B.S. Khakh, T.J. Deming, M.V. Sofroniew, Astrocyte scar formation aids central nervous system axon regeneration, Nature 532 (7598) (2016) 195–200.
[48] M.K.E. Schafer, I. Tegeder, NG2/CSPG4 and progranulin in the posttraumatic glial scar, Matrix Biol. 68-69 (2018) 571–588.
[49] O. Bukalo, M. Schachner, A. Dityatev, Modification of extracellular matrix by enzymatic removal of chondroitin sulfate and by lack of tenascin-R differentially affects several forms of synaptic plasticity in the hippocampus, Neuroscience 104 (2) (2001) 359–369.
[50] M. Geissler, C. Gottschling, A. Aguado, U. Rauch, H.C. Wetzel, H. Hatt, A. Faissner, Primary hippocampal neurons, which lack four crucial extracellular matrix molecules, display abnormalities of synaptic structure and function and severe deficits in perineuronal net formation, J. Neurosci. 33 (18) (2013) 7742–7755.
[51] S. Berretta, H. Pantazopoulos, M. Markota, C. Brown, E.T. Batzianouli, Losing the sugar coating: potential impact of perineuronal net abnormalities on interneurons in schizophrenia, Schizophr. Res. 167 (1–3) (2015) 18–27.
[52] M. Karetko-Sysa, J. Skangiel-Kramska, D. Nowicka, Disturbance of perineuronal nets in the perilesional area after photothrombosis is not associated with neuronal death, Exp. Neurol. 231 (1) (2011) 113–126.
[53] F. Fluri, M.K. Schuhmann, C. Kleinschnitz, Animal models of ischemic stroke and their application in clinical research, Drug Des. Devel. Ther. 9 (2015) 3445–3454.
[54] K. Takano, T. Tatlisumak, A.G. Bergmann, D.G. Gibson Iii, M. Fisher, Reproducibility and reliability of middle cerebral artery occlusion using a silicone-coated suture (Koizumi) in rats, J. Neurol. Sci. 153 (1) (1997) 8–11.
[55] Y. Hase, L. Craggs, M. Hase, W. Stevenson, J. Slade, D. Lopez, R. Mehta, A. Chen, D. Liang, A. Oakley, M. Ihara, K. Horsburgh, R.N. Kalaria, Effects of environmental enrichment on white matter glial responses in a mouse model of chronic cerebral hypoperfusion, J. Neuroinflammation 14 (1) (2017) 81.
[56] H. Taniguchi, K. Andreasson, The hypoxic-ischemic encephalopathy model of perinatal ischemia, J. Vis. Exp. (21) (2008).
[57] S. Bittner, T. Ruck, M.K. Schuhmann, A.M. Herrmann, H. Moha Ou Maati, N. Bobak, K. Gobel, F. Langhauser, D.

Stegner, P. Ehling, M. Borsotto, H.C. Pape, B. Nieswandt, C. Kleinschnitz, C. Heurteaux, H.J. Galla, T. Budde, H. Wiendl, S.G. Meuth, Endothelial TWIK-related potassium channel-1 (TREK1) regulates immune-cell trafficking into the CNS, Nat. Med. 19 (9) (2013) 1161–1165.

[58] S.Y. Kim, V.V. Senatorov Jr., C.S. Morrissey, K. Lippmann, O. Vazquez, D.Z. Milikovsky, F. Gu, I. Parada, D.A. Prince, A. J. Becker, U. Heinemann, A. Friedman, D. Kaufer, TGFbeta signaling is associated with changes in inflammatory gene expression and perineuronal net degradation around inhibitory neurons following various neurological insults, Sci. Rep. 7 (1) (2017) 7711.

[59] H. Kawano, J. Kimura-Kuroda, Y. Komuta, N. Yoshioka, H.P. Li, K. Kawamura, Y. Li, G. Raisman, Role of the lesion scar in the response to damage and repair of the central nervous system, Cell Tissue Res. 349 (1) (2012) 169–180.

[60] J.C. Zbesko, T.V. Nguyen, T. Yang, J.B. Frye, O. Hussain, M. Hayes, A. Chung, W.A. Day, K. Stepanovic, M. Krumberger, J. Mona, F.M. Longo, K.P. Doyle, Glial scars are permeable to the neurotoxic environment of chronic stroke infarcts, Neurobiol. Dis. 112 (2018) 63–78.

[61] B.C. Nolting, K.C. Abbott, Balls, cups, and quasi-potentials: quantifying stability in stochastic systems, Ecology 97 (4) (2016) 850–864.

[62] T.F. Freund, I. Katona, Perisomatic inhibition, Neuron 56 (1) (2007) 33–42.

[63] A. Shah, D.J. Lodge, A loss of hippocampal perineuronal nets produces deficits in dopamine system function: relevance to the positive symptoms of schizophrenia, Transl. Psychiatry 3 (2013), e215.

[64] T. Voigt, T. Opitz, A.D. de Lima, Synchronous oscillatory activity in immature cortical network is driven by gabaergic preplate neurons, J. Neurosci. 21 (22) (2001) 8895–8905.

[65] M. Ayodele, S. Koch, Ischemic preconditioning in the intensive care unit, Curr. Treat. Options Neurol. 19 (6) (2017) 24.

[66] Z. Yao, C. You, M. He, Effect and feasibility of therapeutic hypothermia in patients with hemorrhagic stroke: a systematic review and meta-analysis, World Neurosurg. 111 (2018) 404–412.

[67] M. Haghani, S. Keshavarz, M. Nazari, A. Rafati, Electrophysiology of cerebral ischemia and reperfusion: first evidence for the role of synapse in ischemic tolerance, Synapse 70 (9) (2016) 351–360.

[68] G. Shao, R. Zhang, Z.L. Wang, C.Y. Gao, X. Huo, G.W. Lu, Hypoxic preconditioning improves spatial cognitive ability in mice, Neurosignals 15 (6) (2006) 314–321.

[69] J.T. Neumann, J.W. Thompson, A.P. Raval, C.H. Cohan, K. B. Koronowski, M.A. Perez-Pinzon, Increased BDNF protein expression after ischemic or PKC epsilon preconditioning promotes electrophysiologic changes that lead to neuroprotection, J. Cereb. Blood Flow Metab. 35 (1) (2015) 121–130.

[70] A. McDonough, J.R. Weinstein, Neuroimmune response in ischemic preconditioning, Neurotherapeutics 13 (4) (2016) 748–761.

[71] G. Mukandala, R. Tynan, S. Lanigan, J.J. O'Connor, The effects of hypoxia and inflammation on synaptic signaling in the CNS, Brain Sci. 6 (1) (2016).